Available online at www.sciencedirect.com
SCIENCE DIRECT
Icarus 173 (2005) 559–573
ICARUS
www.elsevier.com/locate/icarus

Sculpting the outer Edgeworth–Kuiper belt: stellar encounter followed by planetary perturbations

M.D. Melita *, J.D. Larwood, I.P. Williams

Astronomy Unit, School of Mathematical Sciences, Queen Mary, University of London, Mile End Road, London E1 4NS, United Kingdom

Received 11 September 2003; revised 28 July 2004

Available online 11 November 2004

Abstract

We consider a close stellar fly-by as an explanation for the abrupt termination of the classical Edgeworth–Kuiper belt at around 50 AU from the Sun, and also for the high values of orbital excitation observed. By the use of numerical simulations we study a scenario in which a close stellar fly-by truncates the trans-neptunian cometary population as a result of strong gravitational perturbations. The results from some representative cases are compared with the presently observed distribution of EKBOs. Our findings suggest that—when observational biases are taken into account—this scenario can reproduce some features of the observed distribution. However, although it is clear that fly-by models are able to generate high values of eccentricity and orbital inclination in the outer particle distribution, this comes at the expense of preserving any low eccentricity particle orbits. The nearly vertical distribution of eccentricities over semimajor axis found at around 48 AU in the EKB cannot be modeled by the use of a stellar fly-by encounter alone. Hence we consider long timescale planetary perturbations and collisional self-interactions that act on the perturbed distribution after a fly-by encounter, and which have the potential to provide a more complete description of the EKBO distribution. However, even when these have been taken into account, the transport of objects from 'hot' to 'cold' orbits may not be sufficient to cover the range of semimajor axes that are observed in the later. Thus, an alternative origin for the low inclination and eccentricity orbits seems likely. The effect of such an encounter on the inner Oort cloud is studied, and we conclude that comets in very large and elongated orbits can be transported to the trans-neptunian region by this mechanism.

Keywords: Trans-neptunian objects, origin; Solar System, comets; Dynamics

1. Introduction

Since the discovery of the first Kuiper-belt object (Jewitt and Luu, 1993) the belt has proved to be full of unexpected features. The initial picture by Kuiper (1950) was of a belt of objects moving on near circular orbits close to the ecliptic, being remnants of the primordial planetesimals that originated in the protosolar nebula. It was soon realized that in addition to this *classical belt*, a large number of the objects were orbiting in mean-motion resonances with Neptune (Williams et al., 1995). Later, a new population was found, composed of objects moving on orbits with large semimajor axes and high eccentricity, now called the *Scattered disk* objects, because it was initially believed that their orbital excitation originated as a result of recurrent close encounters with Neptune (Duncan and Levison, 1997).

The inclination distribution presents another interesting feature, as it has been claimed to be bi-modal (Brown, 2001). When observational biases are taken into account, two populations can be defined, the more inclined 'hot population' (with a mean inclination of 15°) and the more planar 'cold population' (with inclinations smaller than 5°). The numbers of both populations are approximately similar (see Fig. 1). More importantly, the orbital properties of the 'cold' and 'hot' populations correlate distinctively with the surface properties of their members (Tegler et al., 2003; Peixinho et al., 2004). The orbitally cold population is redder than the hot one.

* Corresponding author.
E-mail address: m.d.melita@qmul.ac.uk (M.D. Melita).

0019-1035/$ – see front matter
doi:10.1016/j.icarus.2004.08.020

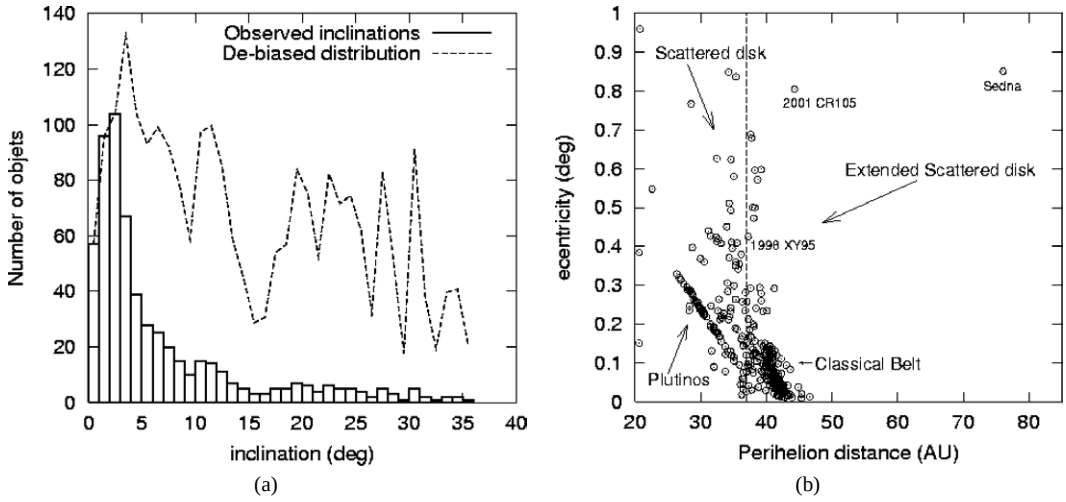

Fig. 1. The Edgeworth–Kuiper belt. (a) Inclination distributions. The broken line indicates the unbiased numbers, which have been obtained by multiplying the distribution by $\sin(i)$ to compensate for the fact that most surveys are performed within a few degrees from the ecliptic (Brown, 2001). (b) The different classes are indicated. The classical belt lies at small eccentricities. The Plutinos lie inside the 2 : 3 mean-motion resonance with Neptune. The scattered disk have large eccentricities and small perihelion distances. The vertical line indicates perihelion distances of 37 AU. It is known (see for example Emel'yanenko et al., 2003) that scattered classical objects will not develop perihelion distances greater than this value under planetary perturbations alone. Thus, this line defines the beginning of the Extended scattered disk.

It is also clear that there is an edge to the classical Kuiper belt (Trujillo and Brown, 2001; Allen et al., 2001). In the classical belt the surface density decreases very steeply ($\propto r^{-11}$, Morbidelli and Brown, 2003) at around 50 AU (see Fig. 1), which leads to the suggestion that the action of an external perturber has truncated the distribution.

A number of hypotheses can be put forward to explain this feature. If the agent responsible were a planetoid, this sudden termination would be the inner edge of a gap, but the observed EKB can hardly be reconciled with such a feature (Melita et al., 2004; Melita and Williams, 2003). On the other hand, the region of the primordial solar nebula—out of which objects as big as we presently observe in the EKB could have been formed—might have been relatively small and sharped-edged itself. Indeed, observed circumstellar disks in star-forming regions appear in a wide range of sizes, from 10 to 1000's AU, and some of them seem also to be sharped-edged (McCaugheran et al., 1998).

A scenario in which the planets are born into a very small protoplanetary disk has been proposed by Levison and Morbidelli (2003). In this case all the presently observed classical-EKBOs would have been formed at heliocentric distances smaller than 35 AU. This scenario can be summarized as follows. When Neptune migrates outwards, EKBO's are captured into its exterior 1 : 2 mean-motion resonance. But the ability to capture resonant objects depends on the *noise* in the evolution of the orbit of the planet (Melita and Brunini, 2000). Thus, in the noisy walk of the 1 : 2 MMR, some EKBO's are left behind in cold orbits. Those EKBOs would be found today in the orbitally-stable classical-EKB.

Close stellar passages are bound to be frequent during the very early life of the Solar System. An evidence that these processes are important is that, although most stars are formed in eccentric binary systems the fraction of binaries decreases over time (Ghez et al., 1997; Kohler and Leinert, 1998), presumably due to dynamical interactions (Kroupa, 1995). Typical separation of binaries are of the order of a few 100 AU's, which set a typical distance for the star close approaches. Indeed, if we assume a star-density as observed in the Trapezium cluster of Orion (Hillenbrand and Hartmann, 1998) and typical relative velocities of a few km/s (Binney and Tremaine, 1987), a few of encounters at 100 AU over the age of the cluster are expected (see also Ida et al., 2000; Kobayashi and Ida, 2001).

It has been suggested that the perturbations given by stellar passages could have excited the first-generation planetesimals, inducing a collisional cascade and preventing further growth in the most affected regions (Kenyon and Bromley, 2002). But such a steep termination as observed is not likely to have been produced by a collisional effects.

Ida et al. (2000) put forward the idea that a close stellar passage will explain both the inclination excitation in the belt and its sudden termination. More recently, Kobayashi et al. (2004) argued that the hot population originates after the encounter from the local objects. Thus, the cold population must be formed independently, i.e., by the 'resonant transport' mechanism (Levison and Morbidelli, 2003). However, in most of the encounters considered, an *outer wing* of large ($a \sim 100$ AU), moderately eccentric orbits ($0.2 \leqslant e \leqslant 0.5$) is generated. No objects belonging to this 'outer wing' has been observed at present. It should be noticed that these orbits do not reach semimajor axes large enough as to coincide with some prominent observed cases, as 2000 CR_{105}, with semimajor axis, $a \approx 227$ AU and perihelion distance, $q \approx 44$ AU or 2003 VB_{12}, with $a \approx 509$ AU and $q \approx 76$ AU (see Fig. 1).

In this investigations, we base ourselves on the star-encounter scenario. We seek to find out if the encounter can

create a sharp edge to the EKB, while solving the problem of the *outer wing* of high-perihelia objects and also understand the origin of orbits as those such as of 2000 CR_{105} and 2003 VB_{12}.

We only consider passages of M-dwarf's, the most abundant type of star in the galaxy. In some exemplary cases, we follow the orbital evolution of the EKB distribution after the encounter, under the perturbations of the 4 major planets. By processing the final result with a survey-simulator, we conclude that the outer wing is mostly precluded from detection due to the observational biases affecting the present sample of EKBOs. On the other hand, a number of particles are left with perihelion distances in the range 37 AU $\leqslant q \leqslant$ 40 AU. These orbits coincide with those of the 'Extended Scatter disk' (see Fig. 1), which cannot be generated by planetary perturbations on their own (see, for example, Emel'yanenko et al., 2003).

On the other hand, we realize that, given the timescale of formation of the EKBOs (Kenyon and Luu, 1999) the stellar encounter is bound to have a major effect on the inner Oort cloud. By the time in which the EKBOs have grown to their present sizes, the inner Oort cloud is mostly formed (see for example Fernandez, 1997). The injection of comets in the planetary region is studied and we conclude that large semimajor axes, large perihelia objects as the ones presently observed (as 2000 CR_{105} and 2003 VB_{12}) can be originated by this mechanism.

In Section 2, we describe the methods used in this investigation. In Section 3, typical end-states of stellar encounters are shown. The effect of the relaxation of the distribution in the presence of planetary perturbations is explored in Section 3.2 where we also discuss the possibility that the cold population derives from the hot one. Bias-corrections are applied to the results an compared with observations. The effect of this type of encounter on the Oort cloud is studied in Section 4. The plausibility of this scenario is discussed in Section 5.

2. Methods

2.1. Stellar encounters

For distant encounters the perturbation follows a power-law that scales as $(a/D)^{3/2}$ for the inclination and as $(a/D)^{5/2}$ for the eccentricity, where a is the semimajor axis of the EKBOs and D is the distance to the perihelia of the passing star. With respect to the perturbing mass it scales as: $M_*/\sqrt{M_*+1}$ (Kobayashi and Ida, 2001). However we are most interested in the outer parts of the disk which are close to the perturbing star, where the perturbation departs from these simple laws. Thus a numerical investigation is necessary to follow the evolution.

We have performed a series of numerical simulations of an encounter between a disk of free test particles orbiting the Sun and a passing star of mass $M_* = 0.3 M_\odot$, corresponding to an M-dwarf, the most common stellar species in the solar neighborhood. As described in Larwood and Kalas (2001), we note that much higher or lower masses do not result in the distant-high eccentric tail of particles that is required here.

We solve the following 3-D equations of motion for the positions of the passing star, $\mathbf{r}_*$, and the EKBO's distance, $\mathbf{r}$, with respect to the Sun:

$$\frac{d^2\mathbf{r}_*}{dt^2} = -G(M_\odot + M_*)\frac{\mathbf{r}_*}{r_*^3},$$
$$\frac{d^2\mathbf{r}}{dt^2} = GM_*\left(\frac{(\mathbf{r}_* - \mathbf{r})}{D^3} - \frac{\mathbf{r}_*}{r_*^3}\right) - GM_\odot\frac{\mathbf{r}}{r^3}, \quad (1)$$

where

$$D = \sqrt{r_*^2 + r^2 - 2\mathbf{r}\cdot\mathbf{r}_*}.$$

The calculations were carried out using a fifth-order Runge–Kutta–Fehlberg integrator with a variable time-step size. This method allows for the fast integration of the motion of $\sim 10^{4-5}$ particles with moderate accuracy. Time-step size control is implemented as described in Press et al. (1992), by specifying a maximum relative error ϵ in the velocity magnitude. The value of ϵ was taken to be as small as practicable (10^{-7}). To prevent too large a reduction in the time-step size owing to close approaches to either of the stellar masses we remove particles from the calculation if they approach either the Sun or the star to within a radius 0.1 of the Sun or a radius 0.01 of the star.

The initial conditions assumed for the passing star are such that it is in a prograde hyperbolic orbit with a given perihelion distance, q_*, inclination i_* and eccentricity e_*. Only runs with argument of perihelion $\omega_* = 90°$ are shown because the dependence of the perturbation on ω_* is weak and, moreover, the eccentricity change of the EKBOs after the passage is greater for this value of ω_*—in the range of inclinations that we are interested in (Kobayashi and Ida, 2001).

Given the form of Eq. (1), the distances can be scaled. The scaling is performed in the following way (see also Kobayashi and Ida, 2001). The heliocentric distances of the particles in dimensionless units, are'expanded' by a factor S. Hence the semimajor axes in Astronomical Units, a, are related to the one in dimensionless unit, a', as: $a = S \times a'$. The value of S is chosen such that the orbital distribution after the encounter would exhibit an edge at $\sim$ 50 AU, roughly reassembling the observed trans-neptunian orbital distribution. Thus, the velocities in astronomical units per year, v, are obtained as: $v = \frac{2\pi}{\sqrt{S}}v'$, where v' is the velocity in dimensionless units.

The perturber was initialized at a distance of ten times the initial outer disk radius (i.e., at 10 units) with a mass of 0.3. We shall consider pericentre distances of $q_* = 2$ and $q_* = 3$. The length and mass units, and therefore the time unit, used in our calculations can be scaled so as to apply to any system within the range of dimensionless parameters that is covered. Thus fixing q_* does not affect the generality of our models and we proceed by scaling distances in an

attempt to correlate features in the final particle distribution with features in the observed distribution of EKB objects.

Throughout we shall use 10^4 test particles initialized in Keplerian circular coplanar (zero inclination) initial orbits, placed at random in the radial interval $0.2R_{\rm out}$ such that the surface density profile decreases according to a power law: $r^{3/5}$. The time unit is such that the orbital period for unit semimajor axis is 2π. The initial outer radius of the disk $R_{\rm out}$ was set to unity, although experiments in varying this parameter were tested, as described later.

2.2. Planetary perturbations

The dynamical relaxation of the orbits of the EKBO's due to planetary perturbations act on timescales that are much longer than the one of the stellar passage, which is of the order of 1000 yr. Thus, to follow the orbital evolution of the EKBO's under the perturbation of the planets a faster method must be used.

The numerical integrator used to compute the planetary perturbations over the age of the Solar System (4.5 Gyr) is a hybrid symplectic second-order method previously used in Brunini and Melita (2002), which treats close encounters with a Burlish–Stoer integrator, in which the strategy developed by Chambers (1999) to preserve its symplectic properties is built in. This method is less accurate than the Runge–Kutta previously used but it still provides reliable results (see for example Brunini and Melita, 2002).

The 4 major planets are included in the simulations. The initial conditions are taken from the output of the chosen stellar encounter simulation. The positions and velocities of 1000 particles are selected randomly from the final dataset such that the semimajor axis distribution is conserved.

3. Results

3.1. Stellar encounters

Our objective is to examine the hypothesis that the overall shape of the observed orbital distribution in the classical EKB is mainly a result of a close stellar passage to the early Solar System. The three major features of the classical EKB to explain are the distributions of inclination, eccentricity, and the steep decline in the number density at around 50 AU (the 'edge').

Runs with varying perturber inclinations (i_*) and eccentricities (e_*) and perihelion distances q_* are shown in Figs. 2, 3, 4 and 5. Notice that the distributions are less steep in the lower e_* model, and note also the large inclinations excited in moderately inclined encounters. These are excited up to the EKB-observed values, $\sim 40°$, for $i_* \leqslant 45°$.

However, in general, the observed distribution is very steep and the outcome of an encounter at a moderate inclination appears depleted of low-eccentricity orbits.

A closer encounter with perihelion distance, $q_* = 2$, eccentricity $e_* = 1$ and inclination $i_* = 30°$, can excite inclinations in the range observed, but at the expense of low eccentricity orbits (see Fig. 2). A less steep eccentricity vs. semimajor axis plot is obtained in an encounter with identical parameters but with an eccentricity of the orbit of the passing star of $e_* = 2$ (see Fig. 3). An even more eccentric encounter $e_* = 3$ would not pump up enough the orbital inclinations of the EKBO's (see Fig. 4). However, a relatively good fit corresponds to an encounter with $q_* = 3$, $e_* = 3$, and $i_* = 45°$ (see Fig. 5).

Thus, orbital excitations as observed in the EKB correspond to encounters with $30° \leqslant i_* \leqslant 45°$ and $1 \leqslant e_* \leqslant 3$. For larger values of e_*, the depletion of low eccentricity orbits is not so severe.

We have scaled some of the models to Solar System units. For these quasi-parabolic moderately inclined encounters, the final inclination distribution of the EKBOs has two 'wings' (see Fig. 6). In the classical belt, inclinations are excited to values as large as 60°. The fraction of objects with inclinations greater than 5° is about $\sim 20\%$ of the total in most of the cases explored.

A large number of objects develop orbits with large semimajor axes (50 AU $< a <$ 100 AU) and perihelia ($q >$ 37 AU) forming an outer wing that is not presently observed (see Fig. 6). These particles originate from the outer parts of the initial disk. When the initial disk is truncated outward of 60 AU, the agreement is found to be much better (see Fig. 7). On the other hand, the possibility that the outer wing could have escaped detection is explored in Section 3.3.

There are many observed objects at semimajor axes ~ 50 AU with perihelia ($q \geqslant 38$ AU), the so-called 'extended' scatter disk. A member of this class, 1998 XY_{95}, is indicated in Fig. 1. These objects are somewhat of a puzzle (see, for example, Collander-Brown et al., 2001) because they could not have developed into those orbits by planetary perturbations alone (Emel'yanenko et al., 2003), thus, these simulations offer a novel explanation for their origin.

3.2. Planetary perturbations

As the initial conditions for computing the planetary perturbations, we have chosen the end-state of a quasi-parabolic encounter with $e_* = 1.01$ and $i_* = 30°$. The initial distribution for the integration of the planetary perturbations is shown in Fig. 6, where the units have been scaled to Solar System units. Notice that the perturbations have to be steep enough as to produce an edge at ~ 50 AU, excite the EKBOs between 40 and 50 AU, but it should be negligible in the planetary region. An inclined encounter (see the corresponding figure for $i_* = 60°$) with a larger star or at a smaller perihelion distance would affect the planetary orbits at a level larger than observed. We have chosen an encounter that produces a very steep plot in the (a, e) plane. Hence, it is better to illustrate the effect of the planetary pertur-

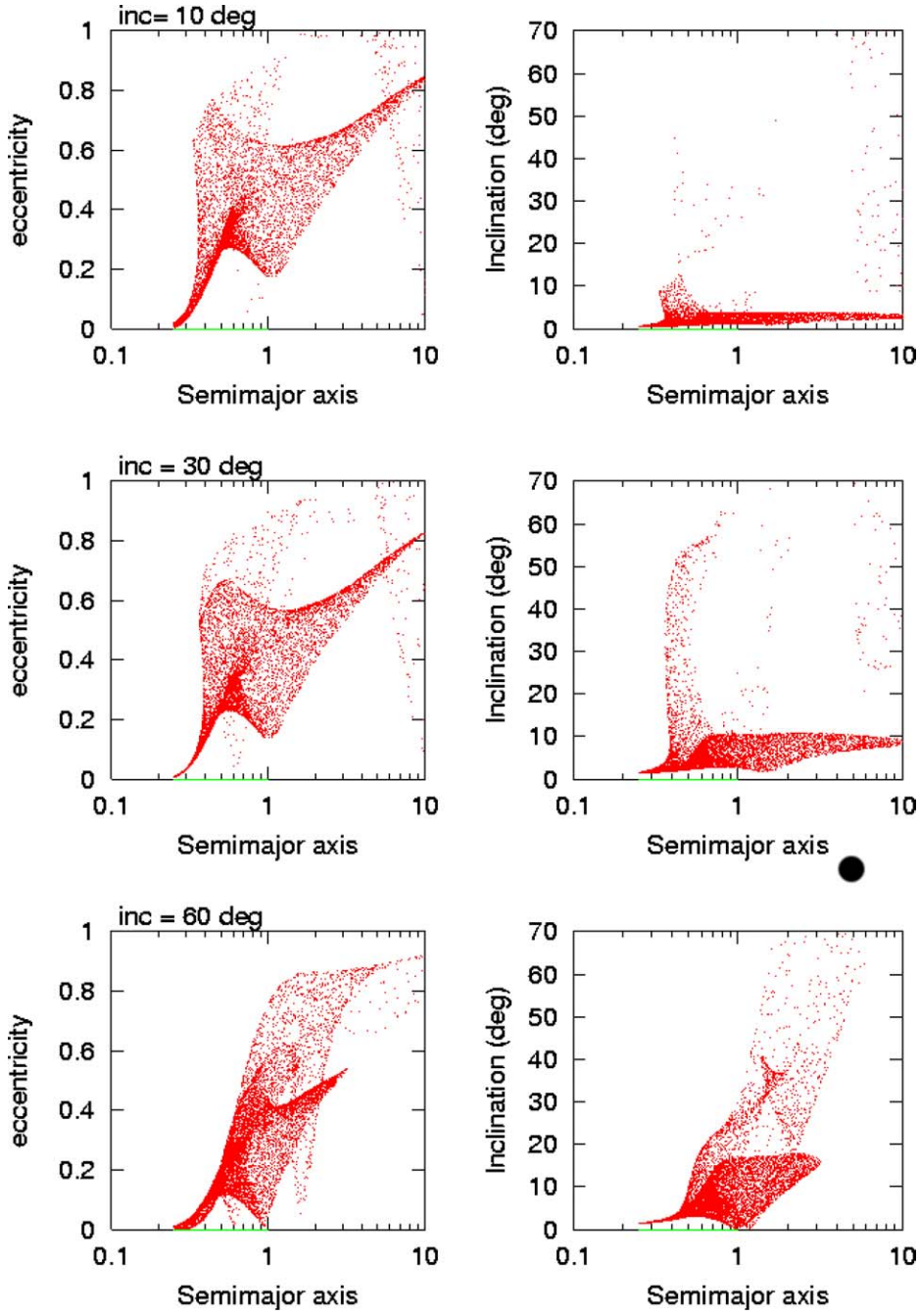

Fig. 2. A plot of eccentricities and inclinations vs. semimajor axis, showing the end-states after the passage of a $M_* = 0.3M_\odot$ star with $e_* = 1.0$, $q_* = 2$ for different inclinations. Inclinations obtained are in the observed range for close-stellar passage with an inclination of 30° to 60°. Low eccentricity orbits are severely depleted.

bations, because the depletion of low eccentricity orbits is greater.

Secular planetary perturbations would produce oscillations in eccentricity and inclinations, while keeping the semimajor axes constant. On the other mean motion resonances produce semimajor axes librations. Also some unstable behavior is expected, with transitions from one regime to the other. We seek to investigate if there are dynamical routes to replenish the region of low eccentricities. We will integrate the orbits of 1000 objects, whose initial conditions are taken from the end-state of a stellar encounter simulation, having scaled the result to Solar System units.

In Figs. 8 and 9 we plot the position of the particles each 10^5 yr in the last 10^8 yr of a 10^9 yr run, the initial conditions were sampled from the distributions shown in Figs. 6 and 7, respectively. We can see that the eccentricity oscillates to low enough values only at discrete locations which correspond to Neptune mean-motion resonances, mainly the 1 : 2, or to secular resonances. Although there is some re-

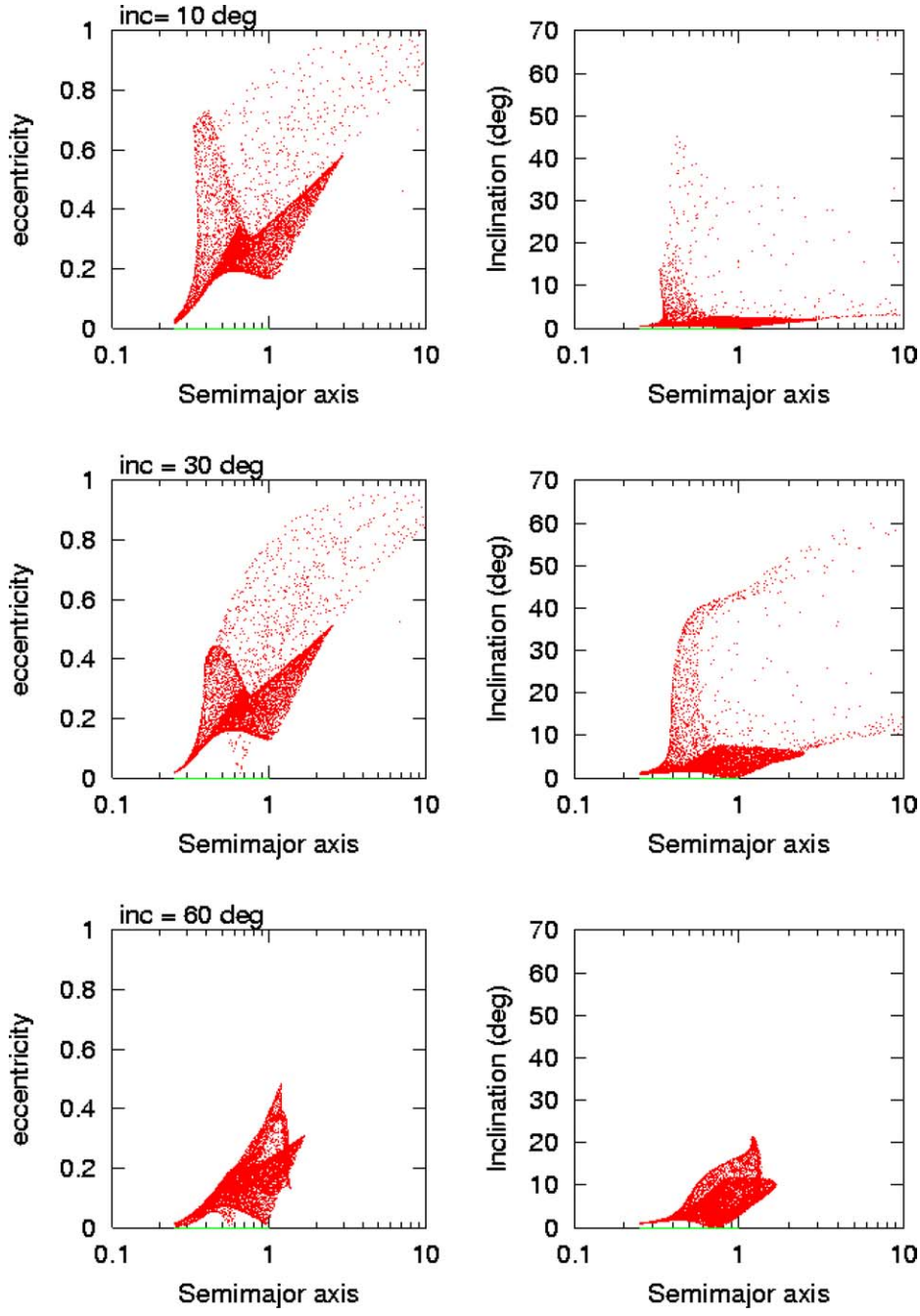

Fig. 3. As Fig. 2 for the passage of a $M_* = 0.3M_\odot$ star with $e_* = 2$, $q_* = 2$ for different inclinations. The largest inclinations are obtained for a close-stellar passage with an inclination of $i_* = 30°$, but low eccentricity orbits are severely depleted.

semblance with the observations, low eccentricity orbits still appear depleted.

Perhaps, further relaxation from self-interactions could replenish cold orbits. An estimate of the effect of physical collisions can be done in the following way. A 100 km EKBO—the typical size of the observed objects, undergoes a few collisions with targets of radii 50 km, over the age of the Solar System, even in the present low density environment (Durda and Stern, 2000). The change in eccentricity, $\Delta e_{\rm coll}$, and semimajor axis, $\Delta a_{\rm coll}$, due to a single collision is given by (see for example Danby, 1962):

$$\Delta e_{\rm coll} = 2\frac{\Delta v_{\rm coll}}{V_K}, \qquad \Delta a_{\rm coll} = 2\frac{\Delta v_{\rm coll}}{GM_\odot} V_K a^2,$$

where $\Delta v_{\rm coll}$ is the velocity change due to the collision, V_K is the local Keplerian velocity and a the semimajor axis of the colliding object. If we take $a = 45$ AU and $\Delta v_{\rm coll}$ as a typical rebound velocity, i.e., the escape velocity of a 50 km icy EKBO, we obtain:

$$\Delta e_{\rm coll} \approx 0.02, \qquad \Delta a_{\rm coll} \approx 0.75 \text{ AU}.$$

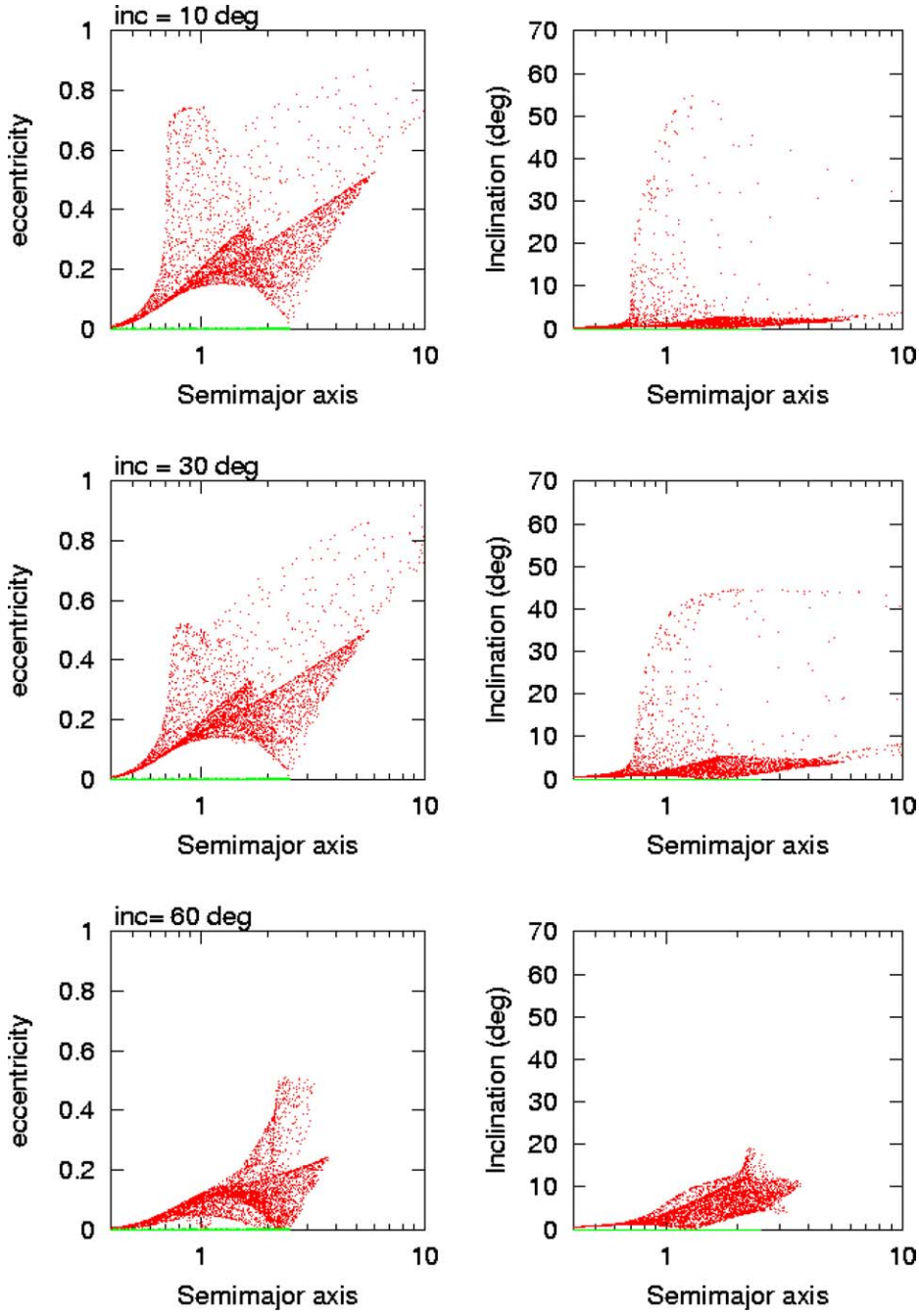

Fig. 4. As Fig. 2 for the passage of a $M_* = 0.3M_\odot$ star with $e_* = 3$, $q_* = 2$ for different inclinations. Again, the maximum inclination excitation corresponds to a close encounter with and inclination $i_* = 30°$, the eccentricity distribution is less steep than in the case with $e_* = 2$.

The width of the 1 : 2 mean motion resonance with Neptune is approximately 1 AU (Melita and Brunini, 2000), thus a single collision can extract an object from the resonance an populate the classical EKB. Similarly objects could escape from secular resonances located between 40 and 42 AU (for the location of secular resonances see Knezévic et al., 1991). But the collisional semimajor axis change seems to be not enough to populate the classical EKB from 40 to 48 AU. On the other hand the eccentricity change is too small as to produce enough collisional diffusion from the 'hot' population into the 'cold' one. Then, it seems unlikely that physical collisions would smear out considerably the distributions given in Figs. 6 and 7, populating the low eccentricity orbits. However this possibility deserves further attention.

3.3. Observational consequences

If the orbital distribution in the EKB were given by the outcome of the previous simulations, what would actually be observed? To answer this question, we have processed the outcome of the previous numerical experiments through

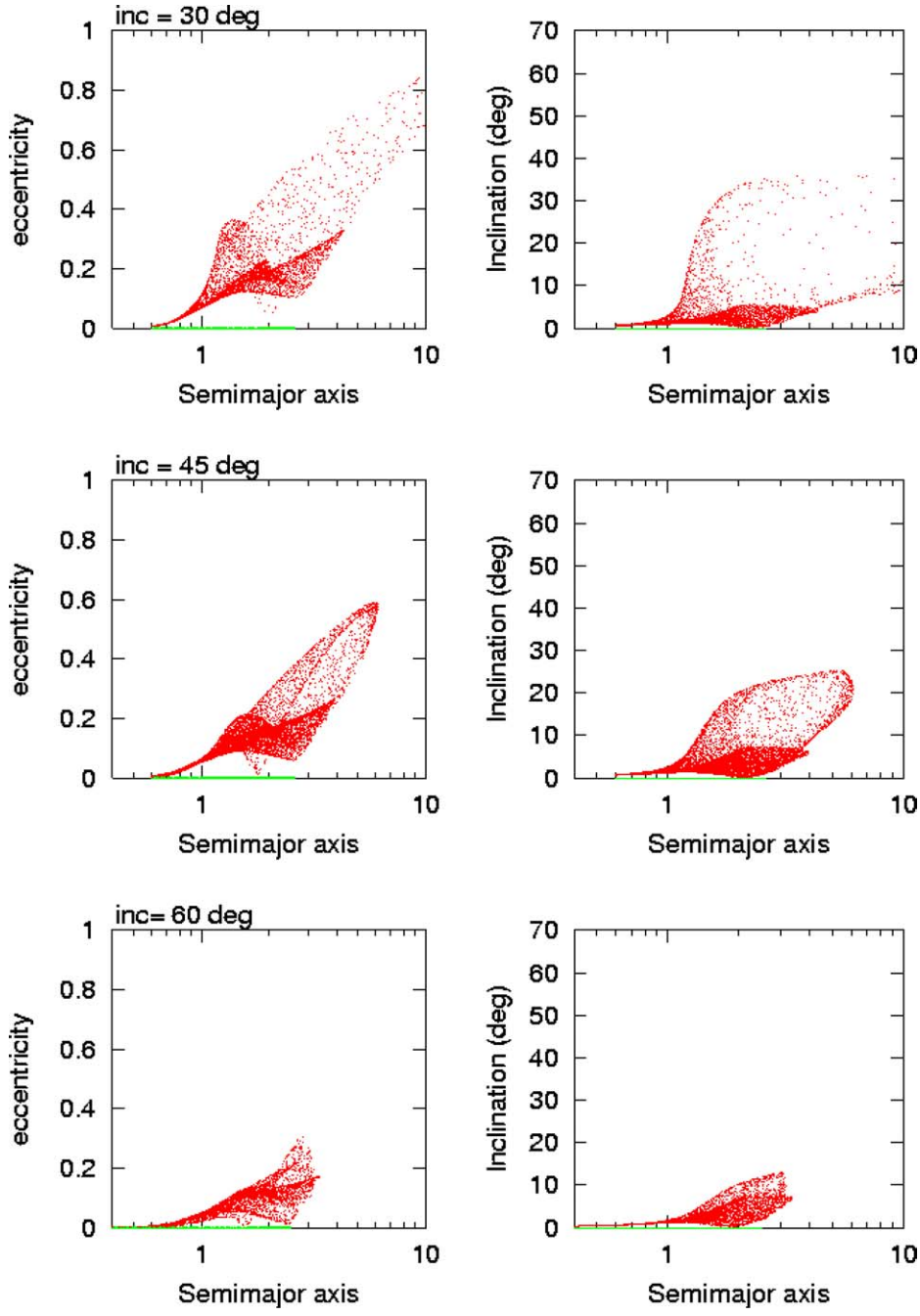

Fig. 5. As Fig. 2 for the passage of a $M_* = 0.3 M_\odot$ star with $e_* = 3$, $q_* = 3$ for different inclinations. The depletion of low eccentricities is not so severe when the inclination of the encounter is $i_* = 45°$. In this case, the excitation of inclinations is just sufficient to explain the observations.

a Survey Simulator, which estimates the distribution of objects that would have been observed at a certain epoch, given the results of a simulation as an input. To build out survey simulator, we have made some simplifying assumptions. We have assumed that all the EKBO discoveries are done within 6° from the ecliptic plane and that the largest red apparent magnitude that can be detected is $m_R = 24.5$. The justification for these assumptions and other details of the Survey Simulator are given in Appendix A. The simulated detections for both the extended and the small initial disk are shown in Figs. 10 and 11, respectively. We have defined a 'vacant region,' where only one object (2003 VB_{12}) has been detected at present as:

$$a \geqslant 50 \text{ AU}, \qquad q \geqslant 45 \text{ AU}.$$

The fraction of objects in the vacant region, f_v, for a smaller initial disk is $f_v = 0$. But for an extended disk the value is $f_v < 0.01$. Thus these results indicate that the outer wing of high perihelia objects at semimajor axes in the range $70 \text{ AU} \leqslant a \leqslant 200$ AU may have well escaped detection at present.

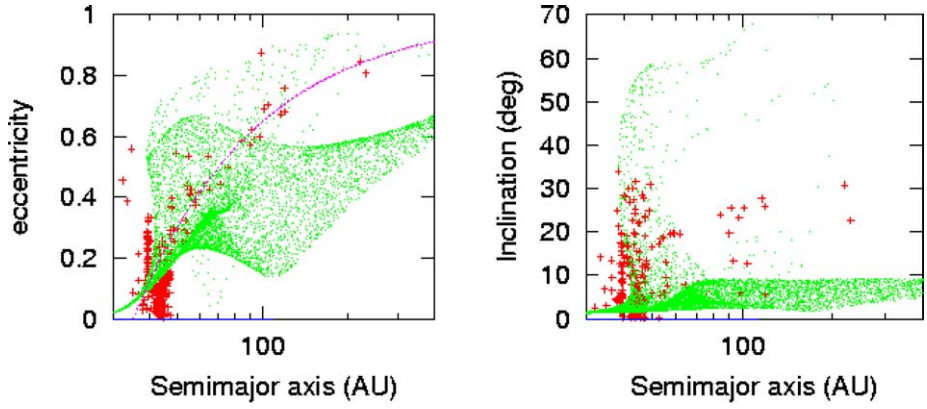

(a) $M = \frac{1}{3} M_{\rm Sun}$, $q = 215$ Au, $e = 1.001$, inc $= 30.0°$

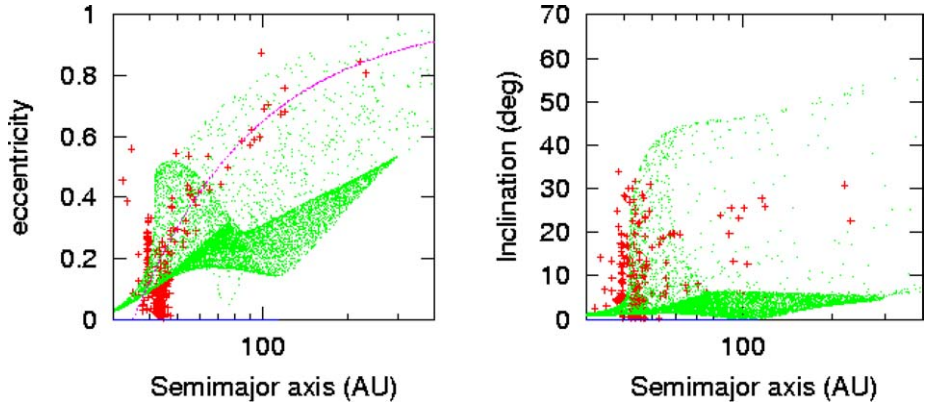

(b) $M = \frac{1}{3} M_{\rm Sun}$, $q = 225$ Au, $e = 2.0$, inc $= 30.0°$

Fig. 6. Final distribution of eccentricities and inclinations vs. semimajor axis in real units (dots). The initial size of the disk is $R_{\rm out} = 105$ AU. The observed multi-opposition objects in the EKB are indicated (crosses). The low eccentricity orbits appear depleted in the classical belt and there is a clear excess of objects at semimajor axes ~ 100 AU and eccentricities $0.2 \leqslant e \leqslant 0.5$. Notice that this 'wing' has mostly low inclinations.

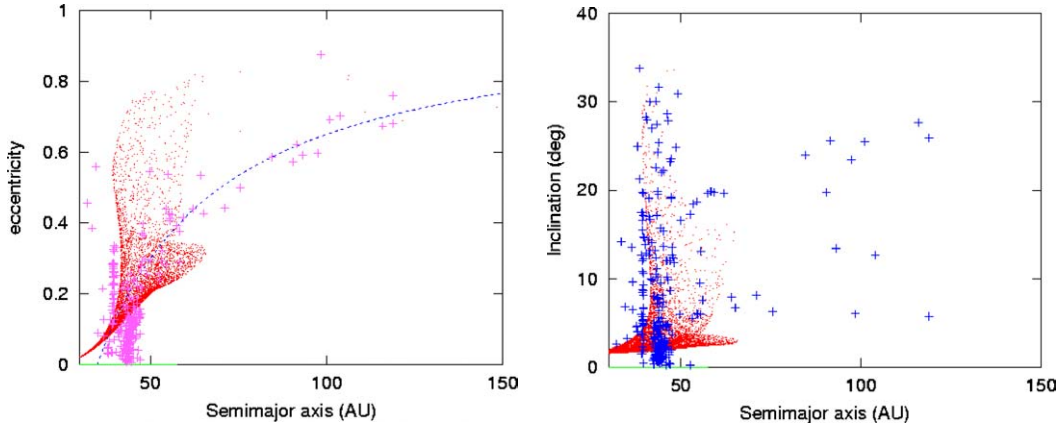

(a) (b)

Fig. 7. As Fig. 6. The initial size of the disk is $R_{\rm out} = 60$ AU. The 'outer wing' at semimajor axes $a \sim 100$ AU is no longer present. Notice that scatter disk objects can originate as a result of close encounters with Neptune. $M = \frac{1}{3} M_{\rm Sun}$, $q = 260$ AU, $e = 1.1001$, inc $= 30.0°$.

4. The effect on the inner Oort cloud

Our current understanding of the origin of the long period comets is that their main reservoir, the inner Oort cloud, is formed in the first few 10^7 yr of the life of the Solar System, when the parental cluster of the Sun was more compact and dense than at present (see, for example, Fernandez, 1997). This explains why the inner Oort cloud is compact itself and located at a few 10^3 AU's from the Sun. Most long period comets are injected into the planetary region from the (outer) Oort cloud—located at 10^4 AU's, formed as a consequence of the outwards diffusion of the more massive inner core.

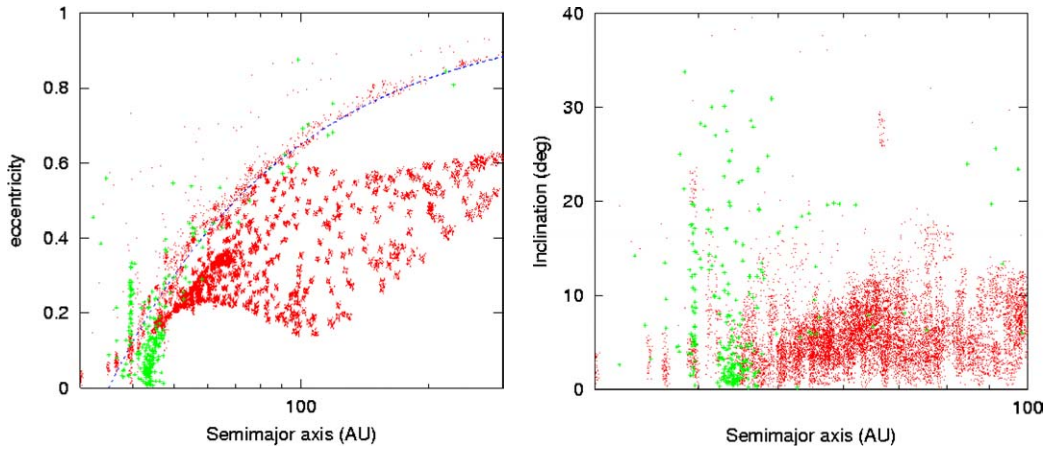

(a) (b)

Fig. 8. Eccentricities and inclinations vs. semimajor axis for positions each 10^5 yr in the last 10^8 yr of a 10^9 yr integration with the major planets. The initial conditions were sampled from the distribution shown in Fig. 6a. The *outer wing* of orbits with large semimajor axes ($a \sim 100$ AU) and moderate eccentricities ($0.2 \leqslant e \leqslant 0.5$) is mostly unaffected by planetary perturbations.

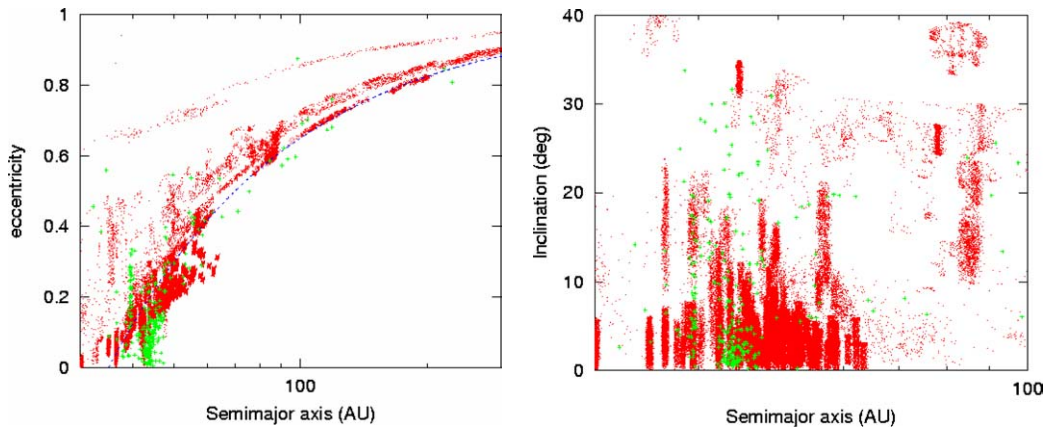

(a) (b)

Fig. 9. Positions each 10^5 yr in the last 10^8 yr of a 10^9 yr integration with the major planets. Eccentricities and inclinations vs. semimajor axis. The initial conditions were sampled from the distribution shown in Fig. 7. The resemblance with the observed distribution is very good, however low-eccentricity orbits still appear depleted.

At the time of the stellar encounter, the cluster is more likely to be still compact, otherwise the probability of such an event would be negligible. But an encounter between a star and the Sun, as the one that we are considering, must happen late in the story of the cluster, after the EKBOs have already formed (Kenyon and Luu, 1999). Thus, such a close encounter is bound to have a major impact on the inner Oort cloud.

For objects close to the Sun (as a EKBO) the direct perturbation on the particle from the star is of similar magnitude than that of the star on the Sun, and a certain cancellation occurs on the perturbing force. On the other hand, if the objects are at a great distance from the Sun in a deeply penetrating encounter into the Solar System, the indirect effect on the Sun predominates, giving rise to a considerable perturbation. A quasi-parabolic encounter with a star of $M_* = 0.3 M_\odot$, results in orbits which are all hyperbolic beyond $a \sim 5000$ AU if the perihelion of the star is at $q_* \sim 200$ AU, even for all planar and circular initial conditions.

The end-state after the encounter for run 4 is shown in Figs. 12 and 13. The fraction of objects that remains bound are shown Table 1 for different initial conditions. Notice that a substantial fraction may survive ($\sim 30\%$), but always a more massive inner Oort cloud must be assumed. Some of the remaining objects are inserted directly into the planetary region and they will be 'rapidly' lost, although this fraction is small $\sim 7\%$.

Notice the existence of objects at perihelia ~ 50 AU and high eccentricities (Fig. 14), these coincide with the orbits of the know objects 2001 CR_{105} and 2003 VB_{12}. The flux of objects from the inner Oort cloud comes into a very wide range of inclinations. That is an artifact of the initial conditions used. If the inner Oort cloud is not entirely thermalized when the objects were inserted into the planetary region, the

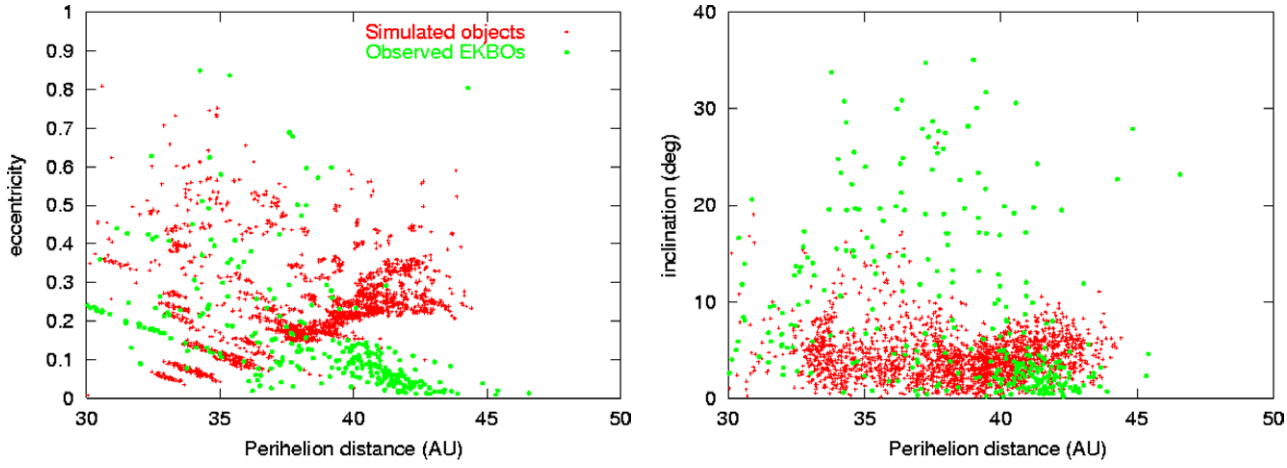

(a) (b)

Fig. 10. Simulated detections for the distribution shown in Fig. 8. Eccentricities and inclinations vs. perihelion distance. The observed objects are indicated (circles).

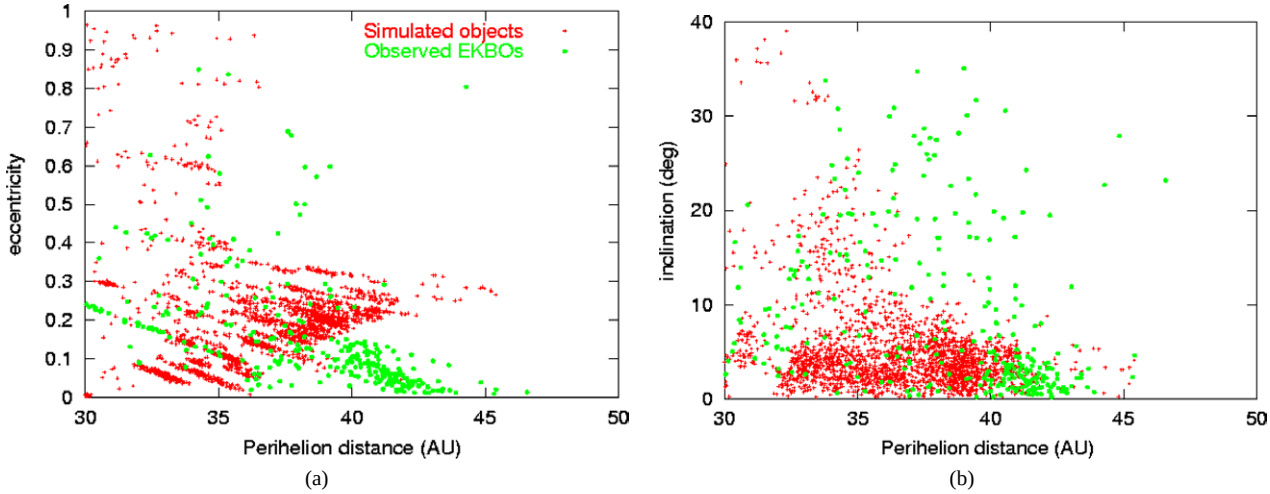

(a) (b)

Fig. 11. Simulated detections for the distribution shown in Fig. 9. Eccentricities and inclinations vs. perihelion distance. The observed objects are indicated (circles).

Table 1
The fraction of objects remaining in bound orbits, f_B, after an encounter with a $M_* = 0.3M_\odot$, $q_* \sim 200$ AU, $e_* = 1.01$, $i_* = 30°$, for different initial conditions

Run	Initial conditions	f_B	f_{sq}
1	$a = U[100\text{ AU}, 50000\text{ AU}]$, $e = U[0, 0.01]$, $i = U[0, \pi]$	7.5	4.8
2	$a = U[100\text{ AU}, 5000\text{ AU}]$, $e = U[0, 0.01]$, $i = E[1000\text{ AU}, 300\text{ AU}]$	33.7	5.1
3	$a = P2[100\text{ AU}, 5000\text{ AU}]$, $e = U[0, 0.01]$, $i = E[1000\text{ AU}, 300\text{ AU}]$	51	6.7
4	$a = U[100\text{ AU}, 5000\text{ AU}]$, $e = G[0.3, 0.3]$, $i = E[1000\text{ AU}, 300\text{ AU}]$	32.0	7.0

The fraction of these with $q < 40$ AU, f_{sq}, is also given. $U[x_{\max}, x_{\min}]$, indicates a uniform distribution between $x_{\max}$ and $x_{\min}$. $P2[x_{\max}, x_{\min}]$ and $P4[x_{\max}, x_{\min}]$ indicate x^{-2} and x^{-4} distributions between those limits, $G[x_{\text{med}}, \sigma]$, a Gaussian distribution with mean x_{med} and standard deviation σ and $E[b1, b2]$ an exponential of the type $\exp((a - b1)/b2)$, where a is the semimajor axis.

inclination distribution of the inner Oort cloud comets inhabiting the trans-neptunian region would span a limited range of inclinations.

It should also be noticed that objects like 2002 VB_{12} can be generated by the *inverse* process, i.e., 'pulled out' from the trans-neptunian region by a close stellar passage (Brunini and Fernandez, 1996).

5. Discussion

We have presented dynamical simulations of the close approach (~ 200 AU) of a $0.3M_\odot$ star to the early Solar System as a model for explaining the major features of the dynamical distribution observed in the present EKB. This model gives best results for a quasi-parabolic ($e_* = 1$–3)

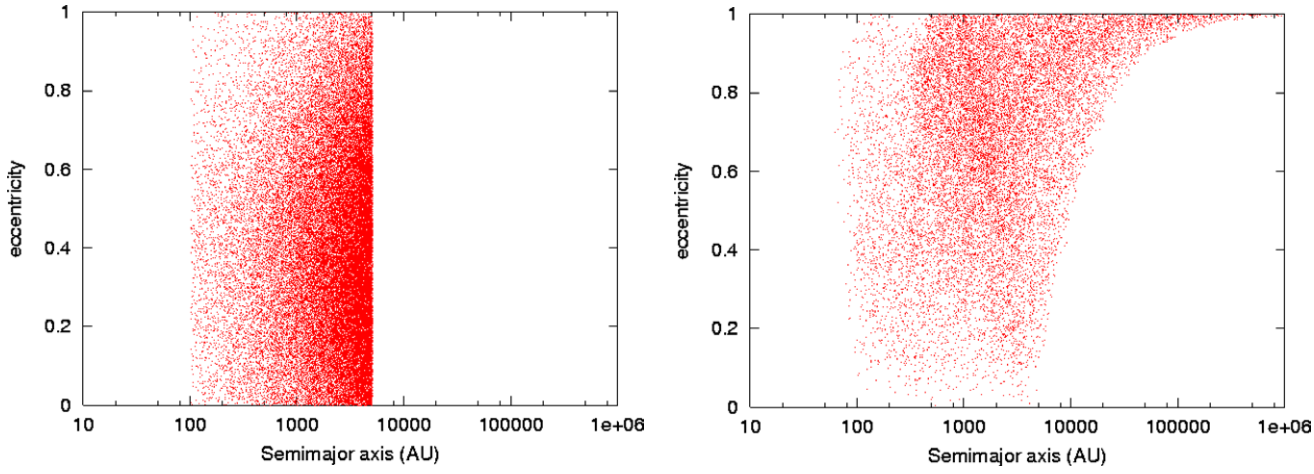

Fig. 12. Eccentricities (initials: (a), finals: (b)). Result of an encounter with a $0.3M_{\odot}$ star, with $q_* = 200$ AU, $i_* = 30°$, and $e_* = 3$ (run 4).

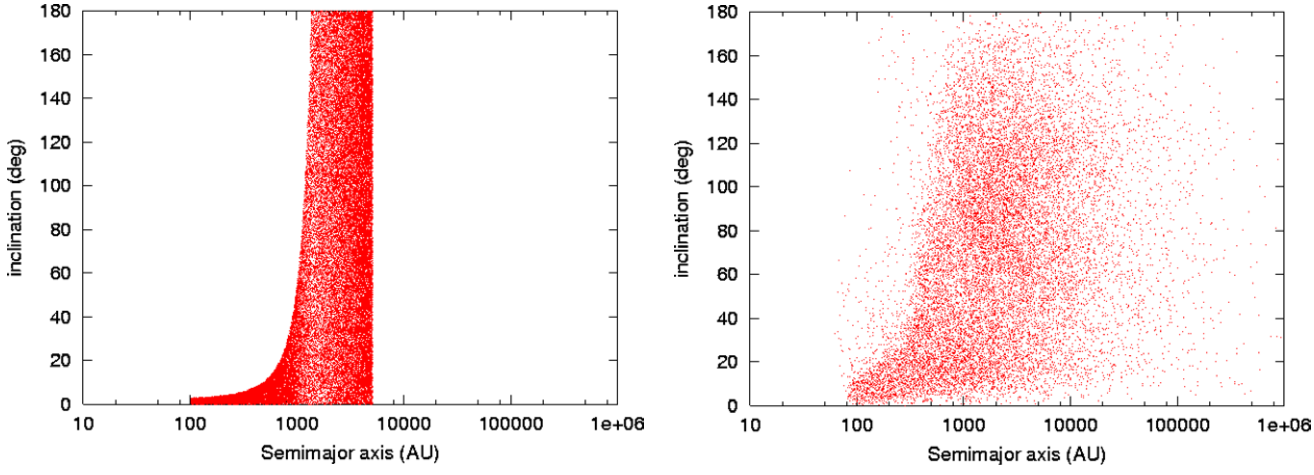

Fig. 13. Inclinations (initials: (a), finals: (b)). Result of an encounter with a $0.3M_{\odot}$ star, with $q_* = 200$ AU, $i_* = 30°$, and $e_* = 3$ (run 4).

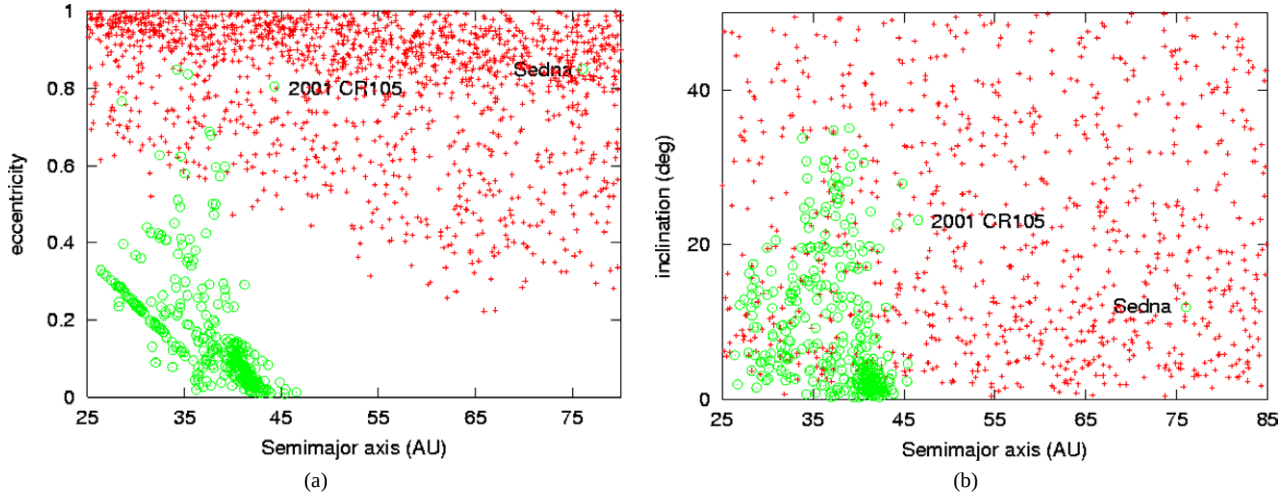

Fig. 14. Comparison between the result of an encounter with a $0.3M_{\odot}$ star, with $q_* = 200$ AU, $i_* = 30°$, and $e_* = 3$ (run 4) and the observed trans-neptunian distribution. The high-perihelia objects 2001 CR_{105} and 2003 VB_{12} (Sedna) are indicated.

encounter at 30°–45° inclination. The steep excitation in eccentricity naturally creates an edge at ∼ 50 AU. Also a group of objects with perihelia 37 AU $\leqslant q \leqslant$ 40 AU is created, which offers an explanation for the origin of the 'extended' Scatter disk.

In the observed sample there are no objects with large semimajor axes (70 AU $\leqslant a \leqslant$ 200 AU) and moderate eccentricities ($0.2 \leqslant e \leqslant 0.5$); in our model such objects originate from particles distributed in the outer parts of the initial disk. Hence it is a prediction of our model that the scattered disk will contain such an 'outer wing.' An object in an eccentric orbit spends most of its time close to aphelion, far away from the Sun. If the orbit is inclined, it would tend to be found away from the ecliptic—or the invariant plane of the Solar System, where most of the surveys have been performed. Thus the probability of detection of this 'outer wing' is very low. If it is eventually determined that those objects do not exist, this may be taken as an indication that the primordial planetesimal disk was small, of the order of 60 AU.

The present model would be untenable if the Sun had formed in a low density stellar environment such as it exists today, since the probability of such a stellar encounter at $q \sim 200$ AU is approximately 0.1% in 100 Myr (Kalas et al., 2000).

The main constraint for the present model is the tight time-window available for the required close encounter to take place. Clearly, the encounter must have occurred *after* the EKBOs were formed: i.e., ∼ 50 Myr after the solar nebula settled into a disk if the objects formed by binary accretion (Kenyon and Luu, 1999). The upper limit is set by the timescale required for the dissociation of the Sun's birth aggregate, generally estimated at ∼ 100 Myr for typical open star-forming clusters. However, if the EKBOs formed by gravitational instabilities in the planetesimal disk (Safronov, 1969; Goldreich and Ward, 1973) then, there is no lower-limit constraint and the stellar encounter can occur at any time in the life of the Sun's parental cluster.

The existence of inner Oort cloud objects in the trans-neptunian region is compatible with the stellar passage scenario since the cometary cloud is severely affected by the encounter. In our model, objects as 2001 CR_{105} and 2002 VB_{12} would not be produced from the trans-neptunian region. But they would be remnants of the early thermalization of the inner Oort cloud produced by the close stellar passage (see Fig. 13).

The close encounter produces a steep orbital excitation. Then the distribution relaxes due to planetary perturbations. These relaxation eliminates objects with perihelia close to Neptune and induces oscillations in inclination and eccentricity. But these are large only at selected locations, such as mean-motion and secular resonances. So the low-eccentricity orbits remain depleted in the classical belt region. We have estimated that the excitation gained at the encounter produces a depletion of cold orbits which cannot be replenished by the effect of physical collisions, even after the relaxation produced by the planets. As suggested by Kobayashi et al. (2004) an alternative origin for the cold population must be sought, which would agree with the latest observational evidence (Tegler et al., 2003).

We also note that the stellar perturbation affects the EKBOs regardless of their physical properties. Hence, it cannot explain directly correlations between the size and dynamics of EKBOs. This problem concerns mainly the alleged correlations between size and inclination, where it has been claimed that the more inclined objects are bigger (Levison and Stern, 2001), although this is not be sustainable in the present sample (Morbidelli and Brown, 2003). On the other hand, correlations between color and orbital excitation (Doressoundiram et al., 2002) may be the result of an indirect effect through collisional processes (Stern, 2002; Gil-Hutton, 2002). However the finding of distinct *groupings* in the surface color of the EKBOs and their correlation with orbital parameters (Tegler et al., 2003), supports the idea that the hot and the cold population do actually have different primordial origins.

Thus, the most likely scenario of the evolution of the EKB derived from our models is that most of the hot population originated from the native objects, excited by the stellar encounter, while the cold population migrated from the inner region.

Acknowledgments

J.D.L. and M.D.M. are funded by PPARC. We are grateful to J. Fernandez and V. Emel'yanenko for useful discussions and to G. Valsechi and H. Kobayashi for providing comments that improved greatly the original manuscript.

Appendix A. The survey simulator

We wish to filter the output of the dynamical simulations through a window that would select objects according to the most relevant biases that affect EKBOs observational surveys. Two main biases are considered, those related with limiting apparent magnitudes and those with ecliptic latitudes.

We take the orbital parameters of the fictitious particles and we calculate the heliocentric and geocentric distances and the sky ecliptic coordinates for a random epoch.

The window that represents the survey simulation eliminates fictitious objects with absolute ecliptic latitudes, δ, greater than 6°. The distribution of δ at discovery of the known trans-neptunian objects is shown in Fig. 15, it is apparent that discoveries at large ecliptic latitudes are very rare.

Then the window eliminates objects with red magnitudes $m_R > 24.5$. The distribution of apparent magnitudes at discovery of the known trans-neptunian objects is also shown

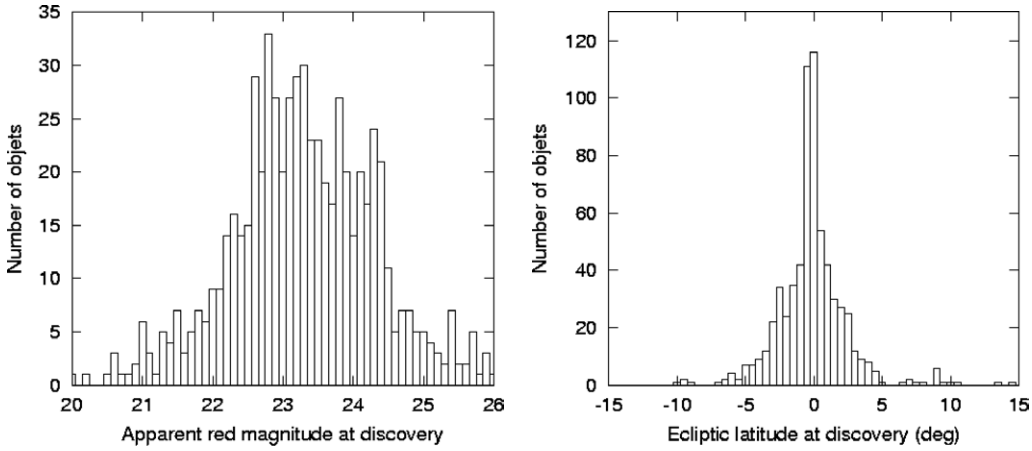

(a) (b)

Fig. 15. (a) Distribution of red apparent magnitudes at discovery of the trans-neptunian objects. Notice the sharp decrease in numbers beyond $m_R = 24.5$. (b) Distribution of ecliptic latitudes at discovery of the trans-neptunian objects. Notice the lack of discoveries al latitudes greater than 6° from the ecliptic.

in Fig. 15, it can clearly be seen that it is truncated at that value.

The apparent red magnitude is given by:

$$m_R = H_0(p, R) + 5\log(r\Delta),$$

where $H_0(p, R)$ is the absolute magnitude, p is the geometric albedo and R the physical radius of the EKBOs, r is the heliocentric distance, and Δ the geocentric distance. So, we need to assign values of size and albedo to each fictitious particle to estimate the value of m_R. The albedo is assumed uniform and equal to $p = 0.04$.

The size R is assigned using a Monte Carlo method. The size-distribution is assumed to follow a differential law of the form:

$$\frac{dN}{dR} \sim R^{-s}, \tag{A.1}$$

where $s = 4.2$ (Trujillo et al., 2001). The sizes are taken form this distribution, between a minimum value $R_{\min} = 70$ km and a maximum one, $R_{\max} = 1000$ km. These values are approximately equal, respectively, to the smallest and biggest physical radius of the observed EKBOs.

We have taken as input all the instantaneous positions of the fictitious particles at regular intervals of time in the last 100 Myr of the total 1 Gyr of simulated time.

In summary, the fictitious particles that gives ‘detection’ by the survey simulator are those with assigned physical values, such that the following criteria are fulfilled:

$$m_R < 24.5, \qquad \delta < 6^\circ.$$

References

Allen, R.L., Bernstein, G.M., Malhotra, R., 2001. The edge of the Solar System. Astrophys. J. 549 (2), 241–244.

Binney, J., Tremaine, S., 1987. Galactic Dynamics. Princeton Univ. Press, Princeton.

Brown, M.E., 2001. The inclination distribution of the Kuiper belt. Astron. J. 121, 2804–2814.

Brunini, A., Fernandez, J.A., 1996. Perturbations on an extended Kuiper disk caused by passing stars and giant molecular clouds. Astron. Astrophys. 308, 988–994.

Brunini, A., Melita, M.D., 2002. The existence of a planet beyond 50 AU and the orbital distribution of the classical Edgeworth–Kuiper-belt objects. Icarus 160 (1), 32–43.

Chambers, J.E., 1999. A hybrid symplectic integrator that permits close encounters between massive bodies. Mon. Not. R. Astron. Soc. 304, 793–799.

Collander-Brown, S.J., Fitzsimmons, A., Fletcher, E., Irwin, M.J., Williams, I.P., 2001. The scattered trans-neptunian object 1998 XY_{95}. Mon. Not. R. Astron. Soc. 325 (3), 972–978.

Danby, J., 1962. Fundamentals of Celestial Mechanics. Macmillan, New York.

Doressoundiram, A., Peixinio, M., de Bergh, C., Fornasier, S., Theault, C., Barucci, M.A., Veillet, C., 2002. The color distribution in the Edgeworth–Kuiper belt. Astron. J. 124 (4), 2279–2296.

Duncan, M.J., Levison, H.F., 1997. A scattered comet disk and the origin of Jupiter family comet. Science 276, 1670–1672.

Durda, D.D., Stern, S.A., 2000. Collision rates in the present day Kuiper belt and Centaur regions: applications to surface activation and modification on comets, Kuiper belt objects, Centaurs, and Pluto–Charon. Icarus 145, 220–229.

Emel’yanenko, V., Asher, D.J., Bailey, M.E., 2003. A new class of trans-neptunian objects in high-eccentricity orbits. Mon. Not. R. Astron. Soc. 338 (2), 443–451.

Fernandez, J.A., 1997. The formation of the Oort cloud and the primitive galactic environment. Icarus 129, 106–119.

Ghez, A.M., McCarthy, D.W., Patience, J.L., Beck, T.L., 1997. The multiplicity of premain-sequence stars in southern star-forming regions. Astrophys. J. 481, 378.

Gil-Hutton, R., 2002. The diversity among Kuiper belt objects: the collisional surfacing model revisited. Planet. Space Sci. 50 (1), 57–62.

Goldreich, P., Ward, W.R., 1973. The formation of planetesimals. Astrophys. J. 183, 1051–1062.

Hillenbrand, L.A., Hartmann, L.W.A., 1998. Preliminary study of the Orion nebula cluster structure and dynamics. Astron. J. 492, 540.

Ida, S., Larwood, J., Burkett, A., 2000. Evidence for early stellar encounters in the orbital distribution of Edgeworth–Kuiper belt objects. Astrophys. J. 528, 531–536.

Jewitt, D., Luu, J., 1993. Discovery of the candidate Kuiper belt object 1992 QB_1. Nature 362 (6422), 730–732.

Kalas, P., Larwood, J., Smith, B.A., Schultz, A., 2000. Rings in the planetesimal disk of Beta Pictoris. Astrophys. J. 530, L133–L137.

Kenyon, S.J., Bromley, B.C., 2002. Collisional cascades in planetesimal disks I. Stellar flybys. Astron. J. 123, 1757–1775.

Kenyon, S.J., Luu, J.X., 1999. Accretion in the early Kuiper belt. II. Fragmentation. Astron. J. 118, 1101–1119.

Kohler, R., Leinert, C.H., 1998. Multiplicity of T Tauri stars in Taurus after ROSAT. Astron. Astrophys. 331, 977–988.

Knezévic, Z., Milani, A., Farinella, P., Froeschlé, Ch., Froeschlé, C., 1991. Secular resonances from 2 to 50 AU. Icarus 93, 316–330.

Kobayashi, H., Ida, S., 2001. The effects of a stellar encounter on a planetesimal disk. Icarus 153 (2), 416–429.

Kobayashi, H., Ida, S., Tanaka, H., 2004. The evidence of an early stellar encounter in the Edgeworth–Kuiper belt. Icarus. Submitted for publication.

Kroupa, P., 1995. The dynamical properties of stellar systems in the Galactic disc. Mon. Not. R. Astron. Soc. 277, 1507–1521.

Kuiper, G.P., 1950. On the origin of the Solar System. In: Heinek, J.A. (Ed.), Astrophysics. McGraw–Hill, New York, pp. 357–424.

Larwood, J., Kalas, P., 2001. Close stellar encounters with planetesimal disks: the dynamics of asymmetry in the Beta Pictoris system. Mon. Not. R. Astron. Soc. 323, 402–416.

Levison, H.F., Morbidelli, A., 2003. The formation of the Kuiper belt by the outward transport of bodies during. Nature 426 (6965), 419–421.

Levison, H., Stern, S., 2001. On the size dependence of the inclination distribution of the main Kuiper belt. Astron. J. 121 (3), 1730–1735.

McCaugheran, M.J., Chen, H., Bally, J., Erickson, E., Thompson, R., Rieke, M., 1998. High-resolution near-infrared imaging of the Orion 114–426 silhouette disk. Astrophys. J. 492, 157–161.

Melita, M.D., Brunini, A., 2000. Comparative study of mean-motion resonances in the trans-neptunian region. Icarus 147 (1), 205–219.

Melita, M.D., Williams, I.P., Collander-Brown, S.J., Fitzsimmons, A., 2004. The edge of the Kuiper belt: the planet X scenario. Icarus 171, 516–524.

Melita, M.D., Williams, I.P., 2003. Planet X and the extended scatter disk. Earth Moon Planets 92, 447–452.

Morbidelli, A., Brown, M.E., 2003. The Kuiper belt and the priomordial evolution of the Solar System. In: Festou, M., Keller, H.U., Weaver, H.A. (Eds.), Comets II. Univ. of Arizona Press, Tucson, AZ. In press.

Peixinho, N., Boehnhardt, H., Belskaya, I., Doressoundiram, A., Barucci, M.A., Delsanti, A., 2004. ESO large program on Centaurs and TNOs: visible colors—final results. Icarus 170, 153–166.

Press, W.H., Flannery, B.P., Teukolsky, S.A., Vetterling, W.T., 1992. Numerical Recipes. The Art of Scientific Computing. Cambridge Univ. Press, Cambridge.

Safronov, V.S., 1969. Evolution of the Protoplanetary Cloud and Formation of the Earth and Planets. Nauka, Moscow.

Stern, S.A., 2002. Evidence for a collisional mechanism affecting Kuiper belt object colors. Astron. J. 124 (4), 2297–2299.

Tegler, S.C., Romanishin, W., Consolmagno, S.J., 2003. Color patterns in the Kuiper belt: a possible primordial origin. Astrophys. J. 599 (1), 49–52.

Trujillo, C.A., Brown, E., 2001. The radial distribution of the Kuiper belt. Astrophys. J. 554 (1), 95–98.

Trujillo, C.A., Jewitt, D.C., Luu, J.X., 2001. Properties of the trans-neptunian belt: statistics from the Canada–France–Hawaii telescope survey. Icarus 122, 457–473.

Williams, I.P., Fitzsimmons, A., O'Ceallaigh, D.P., Marsden, B.G., 1995. The slow-moving objects 1993 SB and 1993 SC. Icarus 116, 180–185.